JINR Summer Student Program 2015

A Monte Carlo study of some characteristics of the BM@N GEM tracker.

Merzlaya Anastasia
(Saint-Petersburg State University,
Faculty of Physics)

Supervisor: Alexander Ivanovich Zinchenko,
PhD, Leading Researcher

Dubna, Russia. 2015

Abstract

BM@N (Baryonic Matter at Nuclotron) is an experimental setup in the fixed-target hall of Nuclotron to perform a research program focused on the production of strange matter in heavy-ion collisions. In the conditions of extreme density and temperature, hundreds of charged particles are produced. In order to extract information about physics in the experiment, particle tracks should be efficiently reconstructed and their parameters should be determined with high precision.

In this work the detector performance was studied for Monte-Carlo simulated event samples of gold-gold collisions. In particular, track reconstruction efficiency was obtained as a function of particle phase space parameters, and the detector coordinate resolution was determined using two different methods.

1. Introduction

JINR Nuclotron accelerator will provide heavy-ion beams with energies up to 6A·GeV for isospin symmetric nuclei and 4.65A·GeV for Au nuclei. In the central heavy-ion collisions at these energies, the nuclear densities of about four times nuclear matter density can be reached. These conditions are well suited to investigate the equation-of-state of dense nuclear matter, which plays a central role for the dynamics of core collapse supernovae and for the stability of neutron stars. Also the heavy-ion collisions are a rich source of strange particles. The extension of the experimental program is related with the study of in-medium effects for vector mesons and strangeness decaying in hadronic modes [1].

For these tasks, it was proposed to install an experimental setup in the fixed-target hall of Nuclotron with the final goal to perform a research program focused on the production of strange matter in the heavy-ion collisions at beam energies between 2 and 6A·GeV [2].

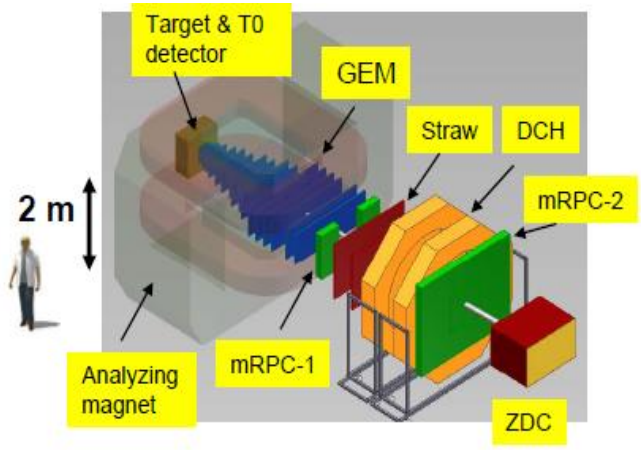

Fig. 1. Schematic representation of BMN.

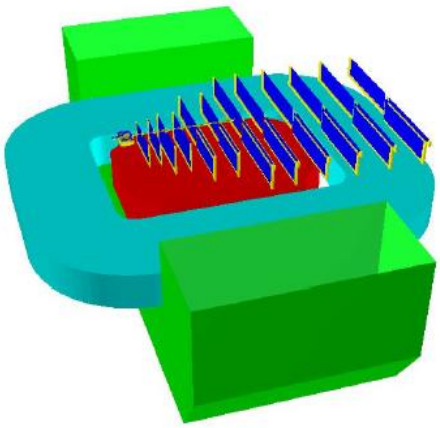

Fig. 2. Schematic representation of inner tracking system.

The general view of the fixed-target detector called "Baryonic Matter at Nuclotron" (BM@N) is presented in Fig. 1. Its detailed description can be found in Refs. [1, 2]. BM@N detector includes a large-acceptance dipole magnet with inner tracking system (Fig. 2), which consists of double-sided silicon-strip sensors and gaseous detectors (GEMs) and has 12 layers. The outer tracking will be based on the time-of-flight system (mRPC), drift chambers (DCH) and zero-degree calorimeter (ZDC).

2. The method of track reconstruction

In the extreme density and temperature conditions realized during the relativistic heavy ion collisions, hundreds of charged particles are produced. In order to extract information about physics in the experiment, particle tracks should be efficiently reconstructed and their parameters should be determined with high precision. Reconstruction of events with high multiplicity is a rather challenging

task. In the BM@N tracking system it is realized within the BMNroot software framework [3].

Track reconstruction in BM@N is based on a combination of the Cellular Automaton and the Kalman Filter methods. The Kalman filter is a recursive filter, which evaluates the state of a linear dynamic system using a set of inaccurate measurements with the errors distributed according to the Gauss distribution [4]. the Kalman filter has two functions: 1) track finding - using information about positions of detector hits it finds track candidates; 2) track fitting – track candidates are fitted to extract track parameters. In order to begin the Kalman filter procedure one needs so-called track seeds, and as one of the possibilities of getting seeds one can take Cellular Automaton method. Cellular automaton is a dynamic method, it evolves in a discrete space consisting of cells [5]. In application to tracking system, connected pairs of detector hits on two consecutive layers can be taken as track segments (cells). So the task of track reconstruction consists of three main steps: formation of tracks-segments, construction of tracks-candidates and track fitting.

3. GEM tracker: phase space

The registration efficiency of the detector depends on its geometrical acceptance and the efficiency of track reconstruction. The geometrical acceptance can be characterized by so-called "reconstructable" tracks, i. e. tracks which presumably should be reconstructed by the track reconstruction method utilized. For the BM@N set-up, these are the tracks passing through at least three consecutive planes of the GEM detectors.

In order to see how tracking efficiency depends on track parameters: total momentum and pseudorapidity (or transverse momentum and rapidity), i.e. the detector phase space coverage, the respective distributions were produced for protons, positively and negatively charged pions for the following track samples:

- Monte-Carlo (MC0) tracks, i.e. all generated tracks;
- Monte-Carlo (MC1) "reconstructable" tracks;
- Reconstructed tracks (STS);
- Reconstruction efficiency obtained by dividing STS by MC1.

It should be noted that the choice of the above-mentioned pairs of parameters is motivated by the fact that the transverse momentum and rapidity are "natural" parameters describing the particle production within the widely used statistical model [6] (and (almost) Lorentz-invariant), while the total momentum and pseudorapidity are more "detector-oriented" values, better characterizing its acceptance.

The phase-space distributions (MC0) for protons, positively and negatively charged pions produced in central Au-Au collisions at kinetic energy 4.5A GeV ($\sqrt{s}$ =3.46A GeV) with the UrQMD event generator [7] are presented in Figs. 3-4, 11-12, 19-20, respectively. The geometrical acceptances (MC1) are shown in Figs. 5-6, 13-14, 21-22 for protons, positively and negatively charged pions,

respectively. Figures 7-8, 15-16, 23-24 respectively present the phase space of reconstructed tracks (STS) for protons, positively and negatively charged pions. The overall detector efficiency for protons, positively and negatively charged pions can be seen in Figs. 9-10, 17-18, 25-26, respectively.

As follows from the figures, the yield of protons is more than two times higher than for positively and negatively charged pions. This fact is in agreement with a statement that in the energy range under study most of the models predict a maximum of the baryon density [1]. Also one can see that the η-p_T distributions for positively and negatively charged pions are almost the same, but the yield of negatively charged pions is approximately 20% larger than for positively charged ones.

After discarding tracks which cannot be reconstructed, the numbers of entries in histograms decrease by approximately one third for pions and one quarter for protons. After the track reconstruction these numbers get reduced by additional 20% for pions and 10% for protons.

According to the figures, most of the tracks in the pseudorapidity region $\eta < 0.8$ cannot be reconstructed, i. e. they do not go into the detector acceptance. There is also a boundary area with $\eta \in (0.8,2)$, where the reconstruction efficiency is relatively low. This region is characterized by a small number of points on tracks and their relatively large polar angle. These features may require a special tuning of the reconstruction algorithm to be properly handled.

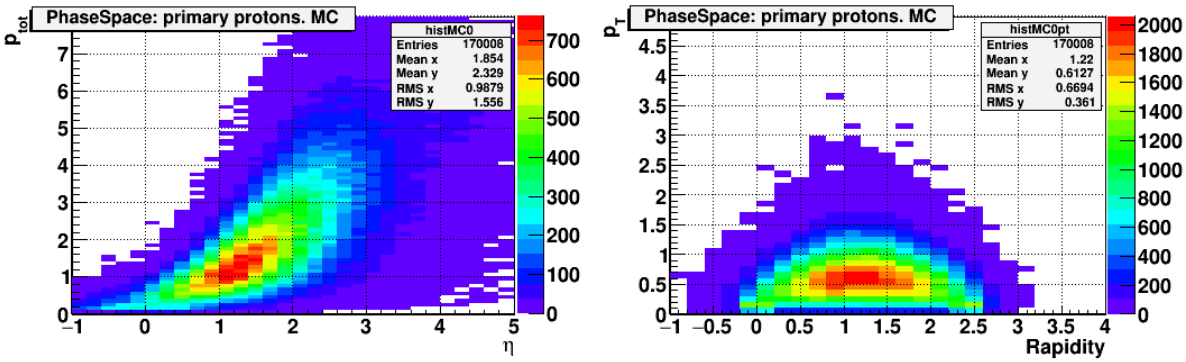

Figs. 3, 4. Phase space of generated protons vs p_{tot}-η and p_T-rapidity.

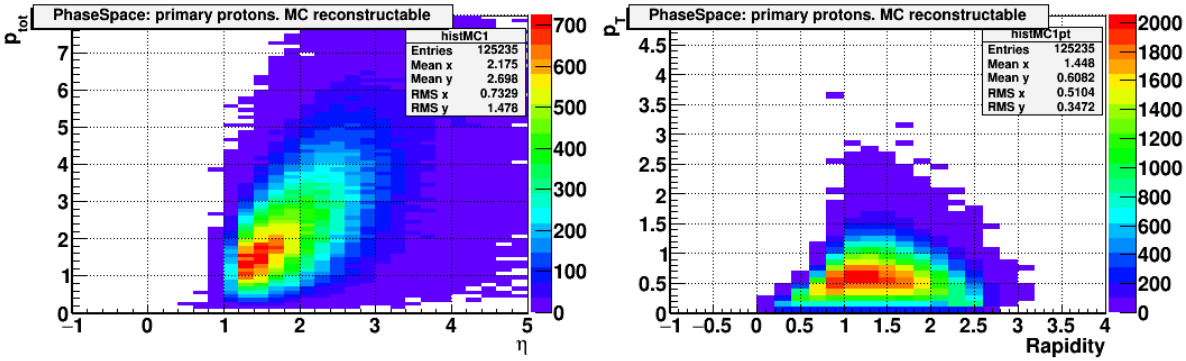

Figs. 5, 6. Phase space "reconstructable" protons vs p_{tot}-η and p_T-rapidity.

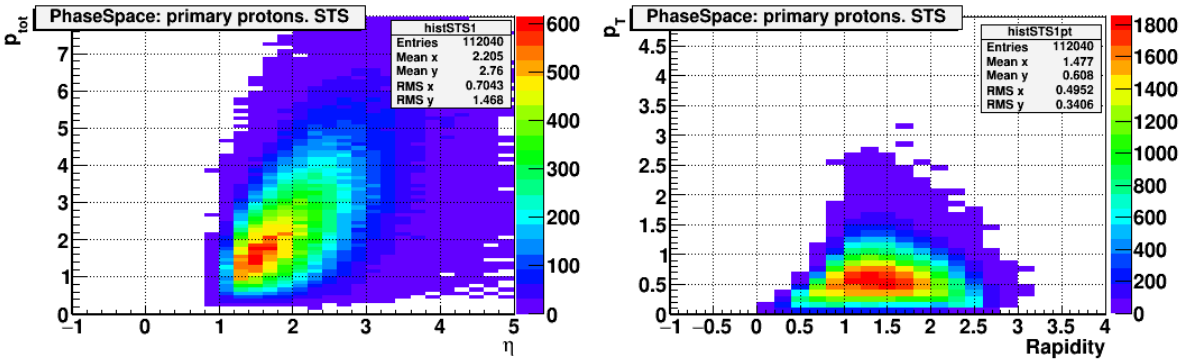

Figs. 7, 8. Phase space reconstructable protons vs p_{tot}-η and p_T-rapidity.

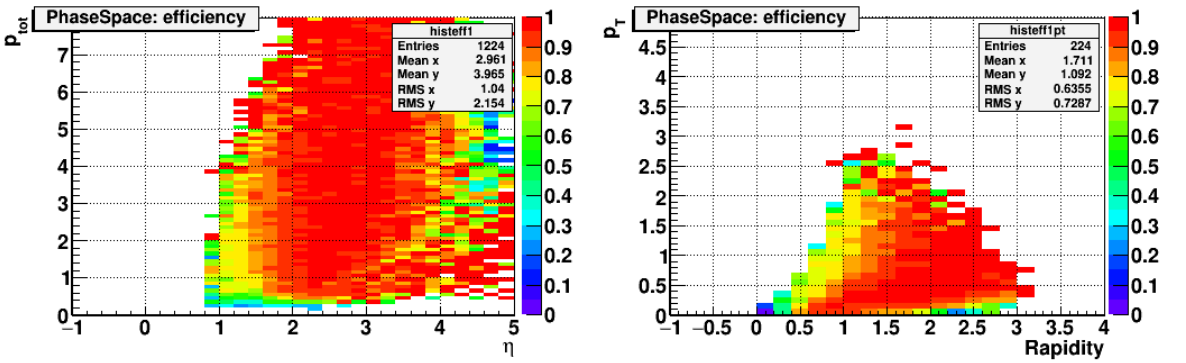

Figs. 9, 10. Proton reconstruction efficiency vs p_{tot}-η and p_T-rapidity.

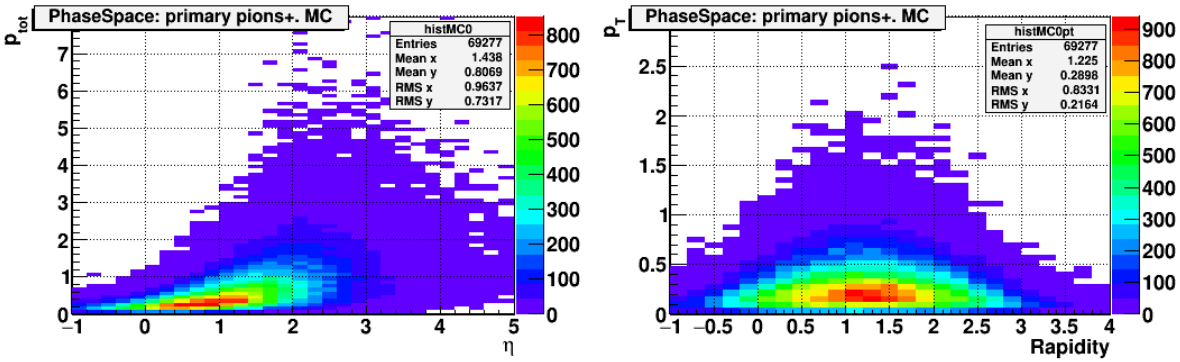

Figs. 11, 12. Phase space of generated positive pions vs p_{tot}-η and p_T-rapidity.

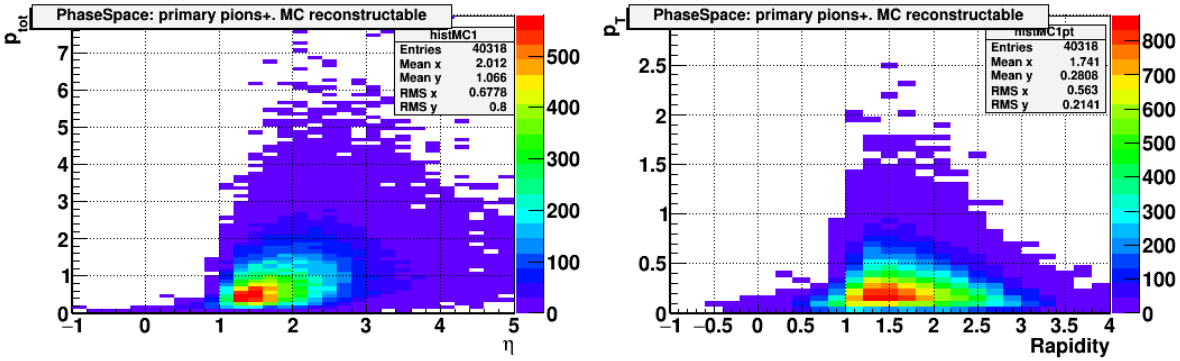

Figs. 13, 14. Phase space "reconstructable" positive pions vs p_{tot}-η and p_T-rapidity.

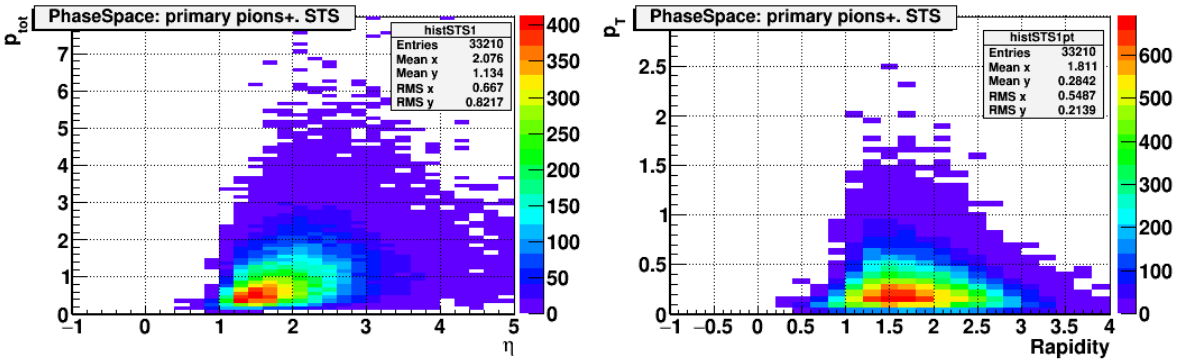

Figs. 15, 16. Phase space reconstructable positive pions vs p_{tot}-η and p_T-rapidity.

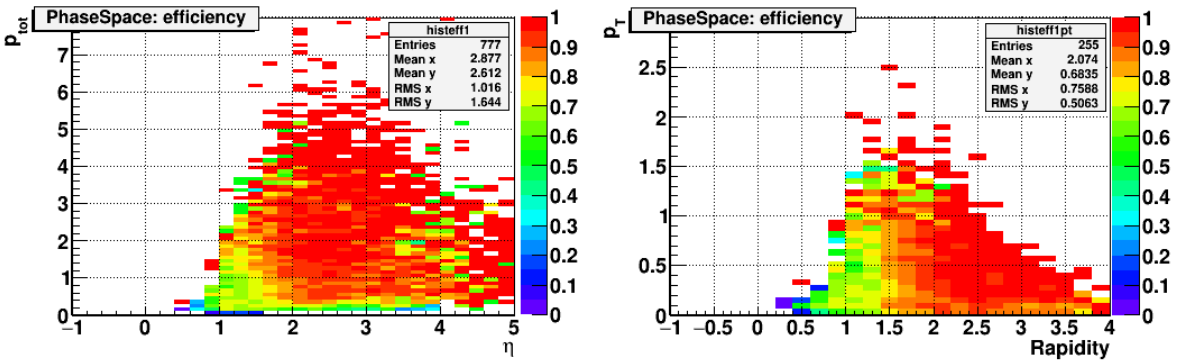

Figs. 17, 18. Positive pion reconstruction efficiency vs p_{tot}-η and p_T-rapidity.

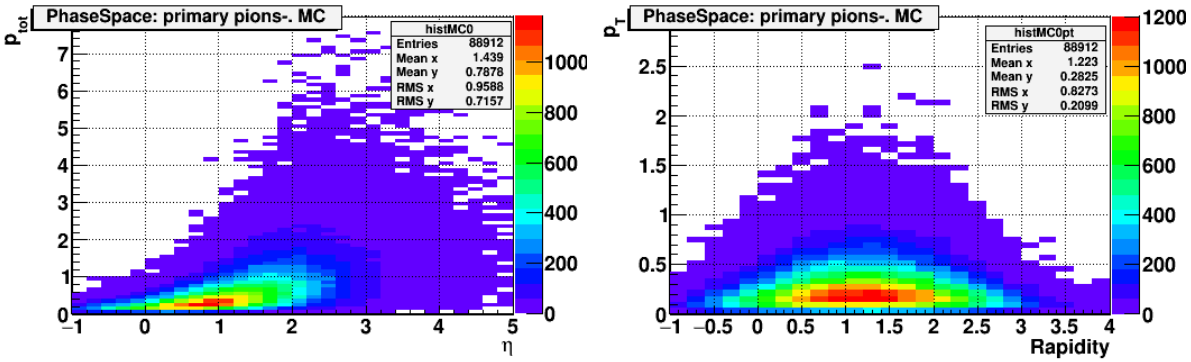

Figs. 19, 20. Phase space of generated negative pions vs p_{tot}-η and p_T-rapidity.

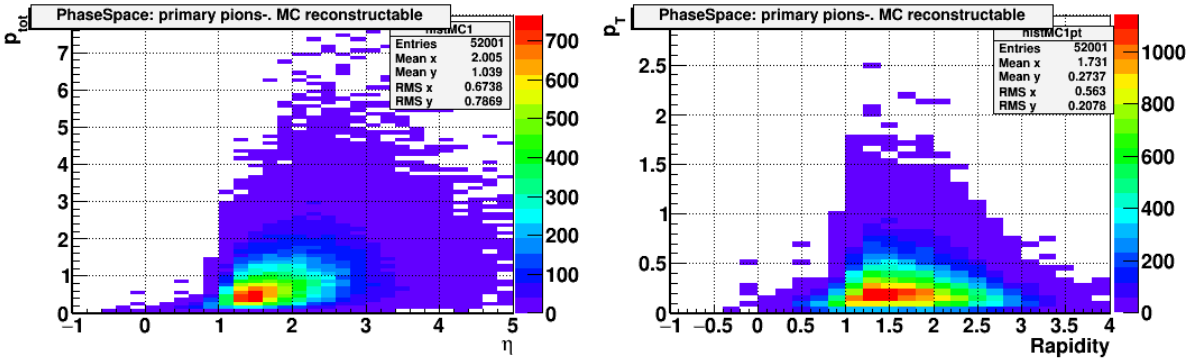

Figs. 21, 22. Phase space "reconstructable" negative pions vs p_{tot}-η and p_T-rapidity.

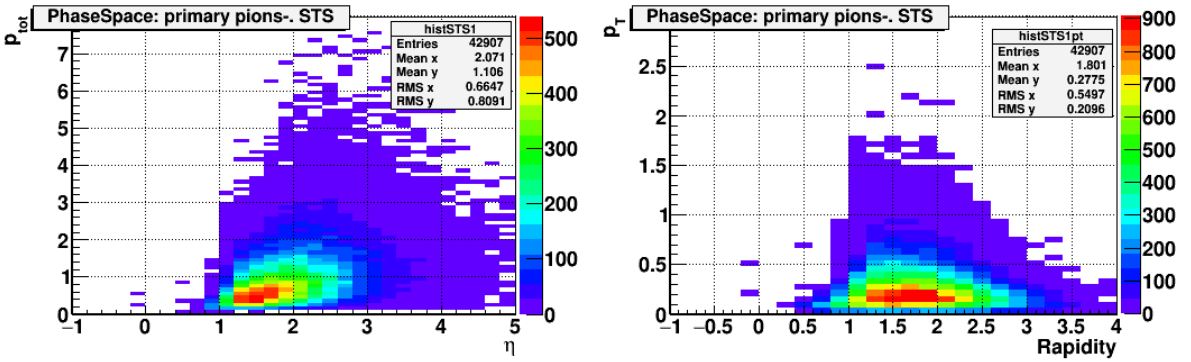

Figs. 23, 24. Phase space reconstructable negative pions vs p_{tot}-η and p_T-rapidity.

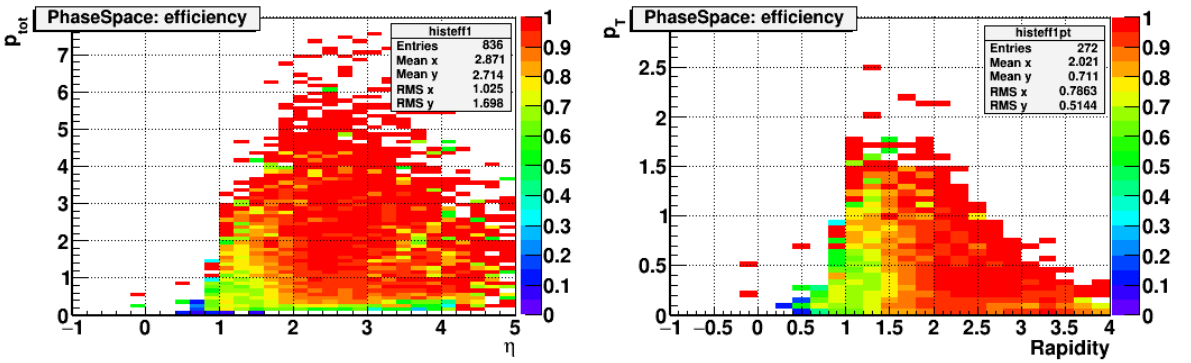

Figs. 25, 26. Negative pion reconstruction efficiency vs p_{tot}-η and p_T-rapidity.

4. GEM tracker: coordinate resolution

In order to determine coordinate resolution of the GEM detectors the following two methods were used. One of the methods is based on a comparison of the reconstructed detector hit positions with the true ones, i.e. the coordinates of particle crossing points with the detector planes (so-called Monte-Carlo points). As such, this method is a purely Monte-Carlo one since true coordinates can be obtained only in simulation. However, it is very useful since a very detailed information is available and can be used to study coordinate reconstruction algorithms in many details. The second method of coordinate resolution extraction can be used in the experiment and is based on a comparison of the reconstructed detector hit positions with the position of the reconstructed track to which the considered hit was assigned.

As a measure of the coordinate resolution the standard deviation (sigma) of the Gaussian fit (1) of the above-mentioned coordinate differences (residuals) was used:

$$f(x) = \frac{1}{\sqrt{2\pi}\sigma} e^{-\frac{(x-x_0)^2}{2\sigma^2}} . \qquad (1)$$

4.1. With Monte-Carlo points

In this method the residual is defined as a distance between a Monte-Carlo point and the nearest reconstructed point, originated from the same particle. The obtained residual distributions along X axis and Y axes were plotted for the first (Figs. 27, 31) and last GEM planes (Figs. 29, 33). One can see on distributions some "shoulders" (black histogram in Figs. 27, 31). It was found that these "shoulders" originated from the divided charge clusters, i.e. large groups of GEM readout strips, containing overlapping charges from several close tracks. In the cluster / hit reconstruction procedure large clusters are divided into several smaller ones, and it looks like this cluster splitting requires some extra tuning.

This observation is further confirmed by Figs. 27, 29, 31, 33 (blue histograms) and 28, 30, 32, 34 where the residuals are shown for “simple” (undivided) and divided clusters. One can see that the simple cluster residuals are closely approximated by the Gaussian function whereas the divided cluster ones have more complicated shape. Obviously, the divided cluster contribution is much higher for the first GEM plane, where track density is quite high, than for the last one (Figs. 28, 30 and 32, 34).

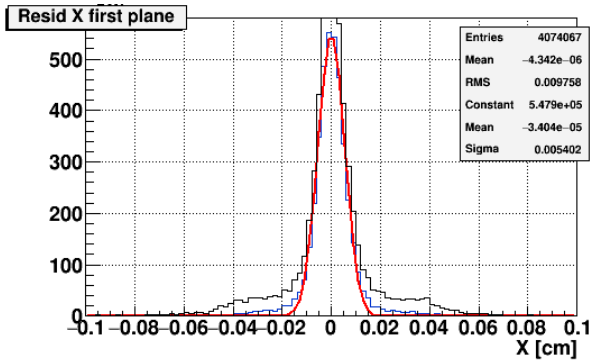

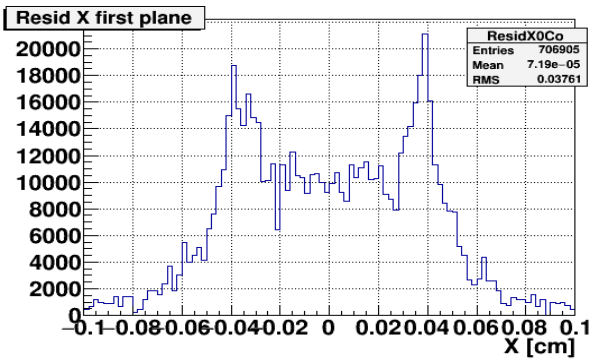

Figs. 27, 28. X-residuals for the first plane for simple clusters and divided ones.

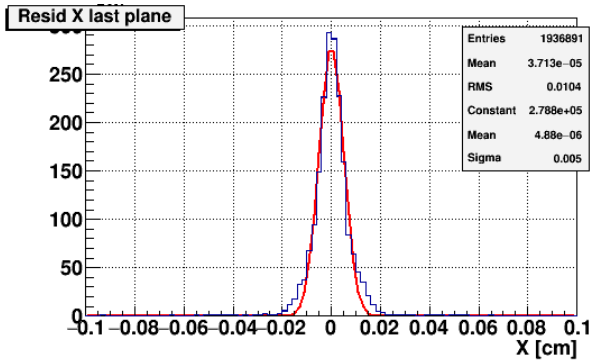

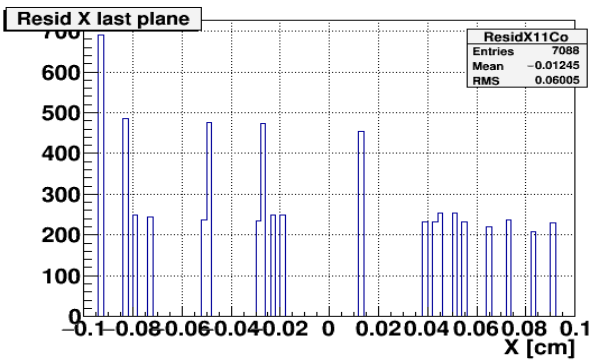

Figs. 29, 30. X-residuals for the last plane for simple clusters and divided ones.

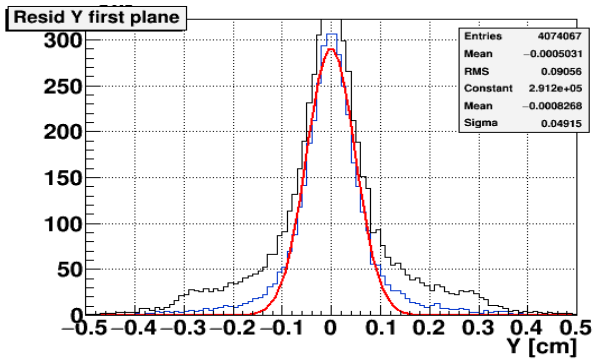

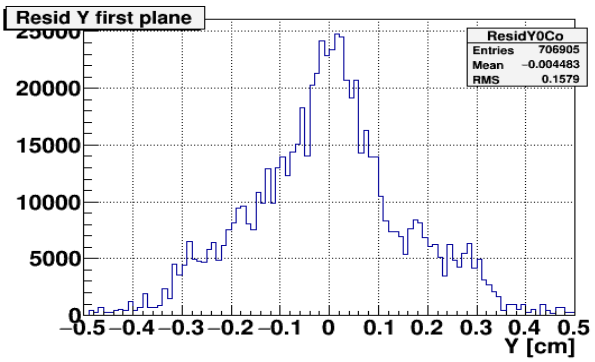

Figs. 31, 32. Y-residuals for the first plane for simple clusters and divided ones.

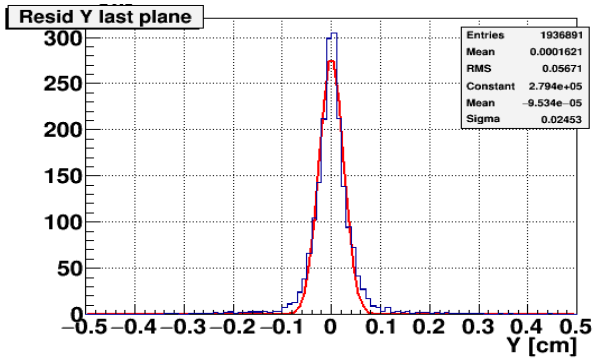

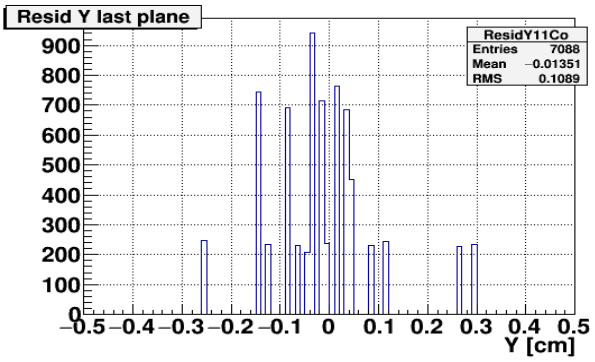

Figs. 33, 34. Y-residuals for the last plane for simple clusters and divided ones.

4.2. With reconstructed tracks

As already stated, in real experiments there is no information about true positions of tracks, passing through detectors, so in order to extract the coordinate resolution of the detector one can look at the position difference between the hit assigned to the reconstructed track and the track itself, i.e. a point on the track on given plane. Since the current implementation of the Kalman filter used for track reconstruction allows to obtain optimal estimates of track parameters only at its ends, the coordinate residuals can be determined for the first and last hits assigned to the track.

The obtained residual distributions along X and Y axes are presented in Figs. 35-38 along with their fits to the Gaussian function for the first and last hits assigned to tracks. Similar distributions in Figs. 39-42 are produced for the hits located at the GEM planes No. 1 and 12. Here the statistics is lower than for the previous sample since not all found tracks start on the plane No. 1 and pass through the plane No. 12.

The obtained results from the both methods are further discussed in Sect. 4.3.

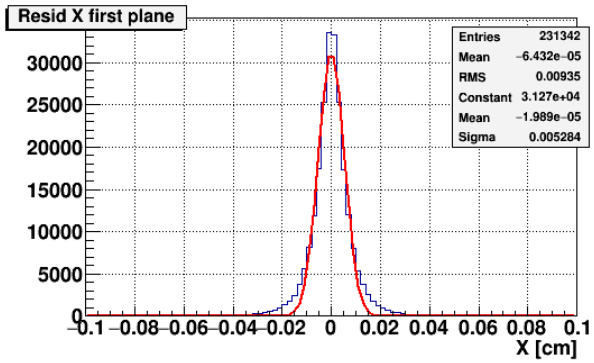

Fig. 35. X-residual for the first hit on track.

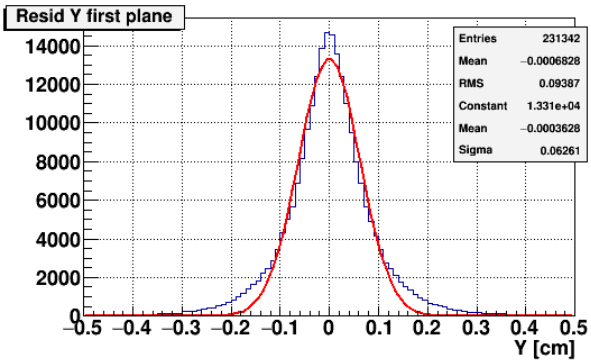

Fig. 36. Y-residual for the first hit on track

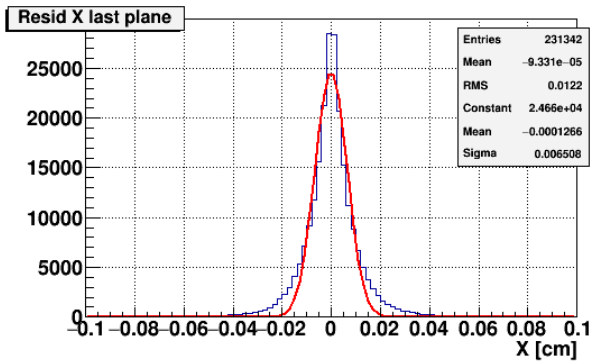

Fig. 37. X-residual for the last hit on track.

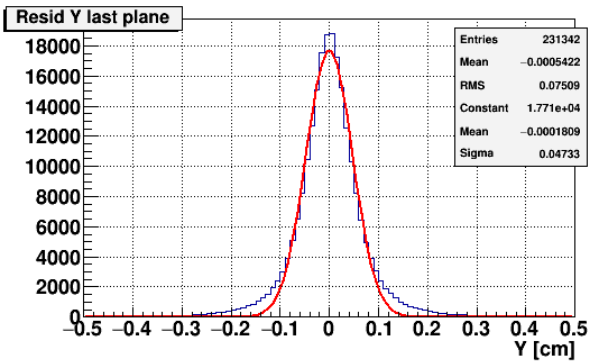

Fig. 38. Y-residual for the last hit on track.

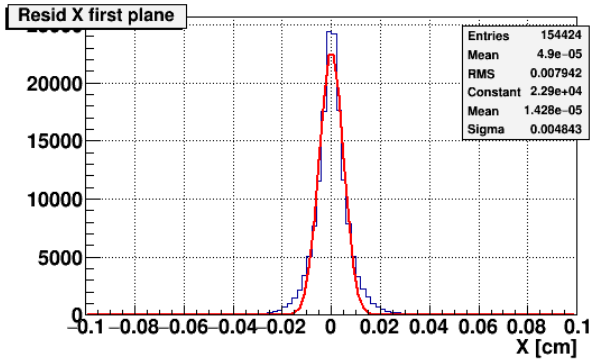

Fig. 39. X-residual for the plane No.1.

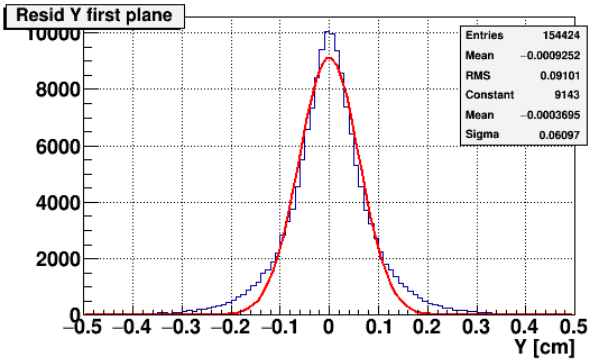

Fig. 40. Y-residual for the plane No.1.

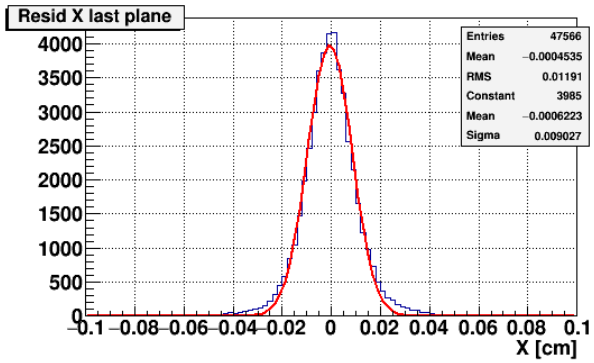

Fig. 41. X-residual for the plane No.12.

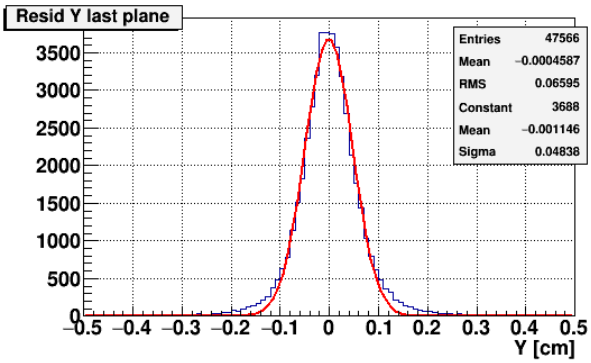

Fig. 42. Y-residual for the plane No.12.

4.3. Both methods: results and discussion

The standard deviations (sigma) of the Gaussian fits for the first and second methods are presented in Table 1, where the first and last planes mean the GEM planes No. 1 and 12. It should be mentioned also that the numbers for the "MC-point" method are the ones for simple clusters. The parameter errors quoted are purely the fit uncertainties and as such they are quite small due to high statistics in the fitted histograms.

Table 1

	With reconstructed tracks	With MC-points
σ_x, the first plane (mm)	0.04843±0.00018	0.05402±0.00003
σ_x, the last plane (mm)	0.0903±0.0004	0.05000±0.00005
σ_y, the first plane (mm)	0.6097±0.0022	0.4915±0.0003
σ_y, the last plane (mm)	0.4838±0.0025	0.24531±0.00023

As the GEMs in the BM@N set-up are double-sided strip detectors two-dimensional position information about hits is derived from two basically one-dimensional measurements obtained by strips on the front and on the back side. Two crossing strips from different sides have a given relative stereo angle that is 7.5° for the first four planes and 15° for the other eight planes and one of the strips oriented vertically. The proper coordinates of a hit in a two-dimensional space

constructed from this overlap of two active strips are the expectation values of the coordinates of the true impact points [8]:

$$\vec{x}_{hit} = \vec{x}\,. \tag{2}$$

Then residuals are given by:

$$\vec{\Delta} = \vec{x}_{\mathrm{hit}} - \vec{x} \tag{3}$$

and their expectation values equal $\vec{\Delta} = 0$.

The error of the measurements is the root of sigma:

$$\begin{aligned} &\sigma^2_{x_{hit}} = \Delta_x^2 - \Delta_x{}^2 = \Delta_x^2 = \\ &= (x - x)^2 = x^2 - x^2 \end{aligned} \tag{4}$$

$$\sigma^2_{y_{hit}} = y^2 - y^2\,. \tag{5}$$

Covariance matrix is given by $\sigma_{x_{hit},y_{hit}} = Cov(x,y)$. In general case if both strips have stereo angles φ_1 and φ_2 with respect to the vertical (y) axis, relation between coordinates on the strips (u,v) and coordinates (x,y) is given by:

$$\begin{aligned} u &= x\cos\varphi_1 + y\sin\varphi_1 \\ v &= x\cos\varphi_2 + y\sin\varphi_2 \end{aligned} \tag{6}$$

Then the inverse transformation will be:

$$\begin{pmatrix} \mathrm{x} \\ \mathrm{y} \end{pmatrix} = R\begin{pmatrix} u \\ v \end{pmatrix}, \tag{7}$$

where transformation matrix is

$$R = \begin{pmatrix} \dfrac{\tan\varphi_2}{\cos\varphi_1\tan\varphi_2 - \sin\varphi_1} & \dfrac{\tan\varphi_1}{\cos\varphi_1\tan\varphi_2 - \sin\varphi_2} \\ \dfrac{1}{\sin\varphi_1 - \cos\varphi_1\tan\varphi_2} & \dfrac{1}{\sin\varphi_2 - \cos\varphi_2\tan\varphi_1} \end{pmatrix}$$

The covariance matrix transforms as

$$\begin{pmatrix} \sigma_x^2 & \sigma_{xy} \\ \sigma_{xy} & \sigma_y^2 \end{pmatrix} = R\begin{pmatrix} \sigma_u^2 & \sigma_{uv} \\ \sigma_{uv} & \sigma_v^2 \end{pmatrix}R^T\,. \tag{8}$$

In our case $\varphi_1 = 0$ and $\varphi_2 = \varphi$ (where $\varphi = 7.5^o; 15^o$), the transformation matrix is

$$R = \begin{pmatrix} 1 & 0 \\ -\dfrac{1}{\tan\varphi} & \dfrac{1}{\sin\varphi} \end{pmatrix},$$

and elements of covariance matrix becomes

$$\sigma_x^2 = \sigma_u^2\,, \tag{9}$$

$$\sigma_y^2 = \frac{\sigma_u^2}{\tan^2\varphi} + \frac{\sigma_v^2}{\sin^2\varphi}\,, \tag{10}$$

$$\sigma_{xy} = -\frac{\sigma_u^2}{\tan\varphi}\,. \tag{11}$$

The error of the measurements for x axis according to (9) is the same as the initial error for strip measurements, i.e. for u axis. This means that residuals for x axis are independent of the stereo angles and should be similar for the first and last

GEM planes. This is consistent with the results for X-residuals in the last column of Table 1.

In (10) the error for y axis has coefficients before errors for u and v axes. The angle φ is small $\varphi \approx 0$, so $\tan\varphi \approx \varphi$ and $\sin\varphi \approx \varphi$. It means that the y-error should be proportional to φ. It is consistent with the results for Y-residuals in the last column of Table 1, where the first and last GEM planes differ by factor of 2 which is exactly the ratio of stereo angles.

Also it is evident from (9) and (10) that the errors of the measurements of y coordinate are much larger than for x coordinate.

In the considerations above it was neglected that the strip pitch in the first four planes was 400 microns as compared to 800 microns in the last eight. Since this difference did not affect the coordinate resolution, one can conclude that the charge distribution on GEM readout planes is much wider than the strip pitch. Actually, the average observed cluster contains 3 strips with a pitch 800 microns. In fact, one can evaluate the expected standard deviation for a Gaussian cluster charge distribution, when the coordinate is reconstructed as a weighted mean. However, this is already beyond the scope of the current investigation.

From Table 1 one can see that both methods give similar errors in X-direction for the first plane while for the last plane reconstructed tracks yield almost twice as large sigma values. This can be explained by the Kalman filter implementation features, namely during the track fitting the procedure assigns to hits the errors as (strip pitch)/$\sqrt{12}$; therefore the last plane uncertainty is overestimated by factor ~2.

As for the Y-errors, the reconstructed tracks method gives values which are not so straightforward to interpret (0.610 mm for the first and 0.480 mm for the last planes). The observed difference with the MC-points method can probably be attributed to the fact that in the Kalman filter implementation Y-coordinate is not taken into account in the explicit form, i.e. different sides of each hit (u and v coordinates) are treated separately during the track fit.

For completeness of information, the residual extraction procedure was repeated for artificial low multiplicity events with particles produced well inside the detector covered phase space, namely 5 positive and 5 negative pions were generated with total momentum p in the interval (0.1;7.0) and pseudorapidity η in the interval (0.5;5) according to Figs. 13 and 21. The Gaussian sigma values for the first and second methods are presented in Table 2.

Table 2

	With reconstructed tracks	With MC-points
σ_x, the first plane (mm)	0.0371±0.0004	0.05231±0.00010
σ_x, the last plane (mm)	0.0734±0.0006	0.05479±0.00014
σ_y, the first plane (mm)	0.415±0.004	0.4399±0.0010
σ_y, the last plane (mm)	0.3717±0.0028	0.2630±0.0007

The obtained values for reconstructed tracks seem to follow the same tendency as in Table 1 being somewhat smaller due to absence of cluster overlapping effects.

5. Conclusion

In this work the detector performance was studied for Monte-Carlo simulated event samples of gold-gold collisions using the BMNroot software framework. In particular, track reconstruction efficiency was obtained as a function of particle phase space parameters for protons and positive and negative pions. Also the detector coordinate resolution was determined using two different methods: with Monte-Carlo points and with reconstructed tracks.

It has been found that some obtained results indicate that additional work on the reconstruction methods is necessary, e.g. improving track reconstruction for low-pseudorapidity region and more detailed study of residual extraction technique using reconstructed tracks.

References

1. Conceptual Design Report. Study of Strange Matter Production in Heavy-Ion Collisions at the Nuclotron. 170pp. http://nica.jinr.ru/files/BM@N/BMN_CDR.pdf
2. BM@N proposal for JINR-PAC Meeting. Study of Strange Matter Production in the Heavy Ion Collisions at Nuclotron. January 10, 2012. 28pp. http://nica.jinr.ru/files/BM@N/BMN_Project_JINR_PAC_Jan2012.pdf
3. BMNRoot. http://mpd.jinr.ru/trac/browser/bmnroot
4. R. Fruehwirth, Application of Kalman filtering to track and vertex fitting, Nuclear Instruments and Methods in Physics Research A 262. 1987. 444-450pp.
5. I. Abt, D. Emeliyanov, I. Kisel, S. Masciocchi, CATS: a cellular automaton for tracking in silicon for the HERA-B vertex detector, Nuclear Instruments and Methods in Physics Research A 489. 2002. 389-405pp.
6. J. Cleymans and K. Redlich, Phys. Rev. Lett. 81 (1998) 5284; Phys. Rev. C 60 (1999) 054908.
7. The Ultrarelativistic Quantum Molecular Dynamics model. http://urqmd.org/
8. V. Karimäki, Hit covariance formalism for stereo detectors, Nuclear Instruments and Methods in Physics Research A 374. 1996. 367-370pp.